

# KINEMATIC CORRIDORS FOR PMHS TESTED IN FULL-SCALE PEDESTRIAN IMPACT TESTS

**Jason R. Kerrigan**  
**Drew B. Murphy**  
**D. Chris Drinkwater**  
**Check Y. Kam**  
**Dipan Bose**  
**Jeff R. Crandall**

University of Virginia Center for Applied Biomechanics  
United States  
Paper Number 05-0394

## ABSTRACT

A primary function of pedestrian dummies is biofidelic representation of whole body kinematics. To assess the biofidelity of a pedestrian dummy, corridors for the kinematic response of post-mortem human surrogates (PMHS) tested in full-scale pedestrian impact tests were developed. Three PMHS were tested in full-scale pedestrian impact tests using a late-model small sedan with an impact velocity of 40 km/h. Three additional tests using the Polar-II dummy were conducted in identical conditions to those used in the PMHS tests.

All impacts were conducted with the PMHS or dummy positioned laterally at the center line of the vehicle, in a mid-stance gait position, with the struck-side limb positioned posteriorly and the upper limbs placed anterior to the torso. Initially supported by a harness, each surrogate was released prior to impact and was unconstrained through a 250 ms interaction with the vehicle.

Using photo targets mounted at the equivalent locations of the head center of gravity (CG), top of the thorax, thorax CG, and pelvis CG, the kinematic response of the pedestrian surrogates was evaluated using parametric trajectory data. To account for simultaneous variability in multiple kinematic parameters, boxed-corridors based on a percentage of trajectory path length were developed from the trajectory data. Given the significance of head impact for pedestrian injury outcome, head velocity-time corridors were also developed.

Comparing dummy response and PMHS corridors, the Polar-II generally replicated the complex kinematics of the PMHS and demonstrated good overall biofidelity. Greater sliding up the hood by the PMHS, and lack of neck muscle tension in the PMHS have been identified as potential causes for differences in the length and shape of body segment trajectories. More testing is necessary to assess the effects differences in pre-test orientation, surrogate stature, and clothing will have on surrogate response.

## INTRODUCTION

Pedestrians killed in pedestrian-vehicle collisions represent 65% of all road traffic fatalities worldwide (World Bank 2001). While the percentage of pedestrian fatalities is much higher in developing nations than in industrialized nations, pedestrians still make up 11%-30% of road traffic fatalities in the US, the European Union, and Japan (NHTSA, 2003, NPA, 2003, CARE, 2002).

To combat this serious public health problem, researchers have been developing pedestrian surrogates like pedestrian dummies and pedestrian computational models to further understand pedestrian injury mechanisms and to evaluate the level of safety afforded to pedestrians by all motor vehicles. Numerous studies presenting data from pedestrian impact tests with different pedestrian dummies were published in the late 1970's and early 1980's. More recently, most of the public research regarding the development and validation of pedestrian dummies has been with regard to one particular dummy, the Polar dummy. Development of the Polar dummies began in the late 1990's by Honda R&D Co., Ltd. in collaboration with GESAC Inc. and the Japan Automobile Research Institute.

The first version of the Polar dummy, the Polar-I, was developed by combining and modifying components from the Hybrid III and THOR dummies (Akiyama *et al.* 1999a and 1999b, Huang *et al.* 1999). Modifications made to the Hybrid III and THOR parts included additional foam in the knee joint flesh, a compliant element in the tibia, and two additional joints to the thoracic/lumbar spine to permit more lateral bending compliance spine. Full-scale tests and component-level tests were performed to assess the biofidelity of the dummy (Akiyama *et al.* 1999a and 1999b, Huang *et al.* 1999).

Based on the results of computer simulations and experiments, modifications to the femur, knee joint and lower extremity flesh were made (Huang *et al.* 1999). An additional series of full-scale pedestrian tests was performed. This new version of the dummy, Polar-I.2,

provided a more biofidelic response than the Polar-I version, but additional improvements were required for biofidelity at vehicle speeds of 32 km/h.

A new version of the dummy, called Polar-II (Figure 1), was developed to improve the kinematic response of the dummy (Akiyama *et al.* 2001). A new knee joint (Figure 1) with human-like geometry and a new flexible tibia were added to improve lower extremity biofidelity. The shoulder joint was also modified to decrease the stiffness for motions within the normal human range. Additionally more instrumentation was added to obtain kinetic data in the lower extremity and deflection data in the thorax and abdomen (Akiyama *et al.* 2001). Full-scale pedestrian impact tests were performed on the Polar-II with six different sized vehicles to further understand how differing vehicle shapes affect pedestrian kinematics (Akiyama *et al.* 2001 and Okamoto *et al.* 2001).



**Figure 1. Polar-II dummy with human-like knee joint inset. (Akiyama, 2001)**

The biofidelity of the Polar dummy has been evaluated by comparing its response in full-scale impact tests to the response of PMHS in similar experiments (Akiyama *et al.* 1999a and 1999b, Huang *et al.* 1999, Akiyama *et al.* 2001). The experiments on the PMHS, discussed in Ishikawa *et al.* (1993), were performed using a similar, not identical, vehicle as the full-scale tests performed using the Polar-II dummy (Akiyama 2001).

Numerous other studies have documented the results of full-scale pedestrian impact testing on hundreds of PMHS. While the previous studies provide valuable information regarding full-scale test methodology, many of the tests were performed on vehicles not representative of the current vehicle fleet (Kam *et al.* 2005). Additionally, many of the previous full-scale impact test studies do not provide kinematics

data in enough detail to permit use of the data in validation studies (Kam *et al.* 2005).

Thus, there is a need for additional study of full-scale pedestrian impact tests on PMHS with late-model vehicles to develop detailed kinematics data. For further assessment of the biofidelity of the Polar-II, full-scale pedestrian impact tests should ideally be performed using identical test conditions so that the Polar-II response can be directly compared to the PMHS response. The goals of this study are threefold:

- to perform full-scale pedestrian impact tests on PMHS with late-model small sedan,
- to develop kinematic response corridors for upper-body trajectories, and
- to evaluate the response of the Polar-II dummy, tested using identical conditions as in the PMHS tests.

## FULL-SCALE TEST METHODOLOGY

Six full-scale pedestrian impact experiments were performed with a small sedan. Three tests were performed using PMHS and three tests were performed using the Polar-II dummy. The test conditions remained identical in all six tests to minimize variability in the results and facilitate a biofidelity evaluation of the Polar-II dummy.

### Sled System

The vehicle used in all six tests was a recent model small sedan. A scaled dimensioned drawing of the center line contour for the front of the vehicle is given in Figure 2. The vehicle was cut in half at the B-pillar and mounted on a sled fit to the deceleration sled system at the UVA Center for Applied Biomechanics. A hydraulic decelerator was positioned at the impact end of the sled tracks to stop the vehicle at the end of the surrogate (dummy or PMHS) interaction.

Since the sled tracks at UVA are above ground, an additional sled was necessary to serve as the ground level surface on which the pedestrian surrogate (PMHS or dummy) would be positioned. Thus a small, light sled was constructed to hold two pieces of plywood used to simulate the ground surface. Plywood has been shown to possess frictional characteristics similar to road surfaces (Kam *et al.* 2005). This “pedestrian sled” was positioned before each test in a location that permitted the vehicle to interact with the pedestrian surrogate for approximately 250 ms between initial bumper contact and vehicle deceleration (Figure 3). For more discussion on why a 250 ms interaction time was chosen, see Kam *et al.* (2005).

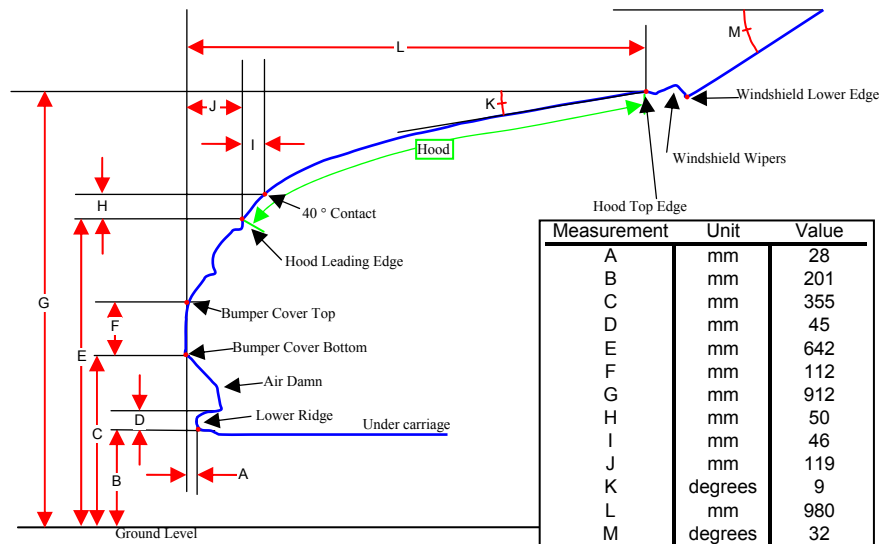


**Figure 2. Scaled, dimensioned drawing of the front of the small sedan used in all tests in the current study.**

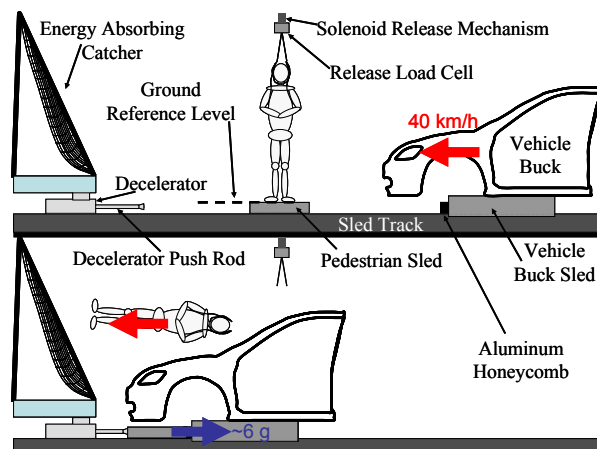


**Figure 3. Schematic of full-scale pedestrian impact test system. Not to scale.**

The primary objective of the current study was to examine only the interaction of the pedestrian and the vehicle. Secondary contact with the ground, road structures or other vehicles was not studied. Therefore an energy-absorbing catching structure was constructed at the impact end of the sled to catch the pedestrian surrogate, and lay it softly on an energy absorbing bed. The purpose of the catching structure was to reduce the potential to cause additional injuries to the PMHS during vehicle deceleration.

During the impact event, the vehicle sled was accelerated to 40 km/h, and it subsequently struck the pedestrian surrogate. Approximately 50 ms later, the vehicle impacted and accelerated the pedestrian sled (Figure 3). By this time, the pedestrian surrogate had long since relinquished contact with the ground level surface of the pedestrian sled. About 250 ms after the

vehicle initially contacted the pedestrian surrogate, the pedestrian sled, now coupled to the vehicle sled, contacted the decelerator, slowing them to a stop at a rate of approximately 6 g. At this time the pedestrian surrogate was lofted forward into the energy absorbing catching structure (Figure 3). For more information regarding the UVA sled system, and how it is configured for full-scale pedestrian collisions, see Kam *et al.* (2005).

### PMHS Preparation

The criteria used to select the three PMHS (Table 1) used in this study include stature, weight, and cause of death. Specimens were chosen that had a stature between 170 and 175 cm, a weight between 50 and 85 kg and a cause of death that didn't involve traumatic injury. Pre-test CT scans were used to confirm the absence of pre-existing fractures, lesions and other bone pathology in all skeletal structures. All PMHS were preserved by a combination of refrigeration and freezing (Crandall, 1994). All PMHS were obtained and treated in accordance with the ethical guidelines approved by the Human Usage Review Panel, National Highway Traffic Safety Administration, and all PMHS testing and handling procedures were approved by the University of Virginia (UVA) institutional review board.

Approximately four days prior to testing, each PMHS was removed from the freezer and allowed to thaw at room temperature over a three day period. Approximately one day before each test, the specimen preparation began. During preparation, a series of hardware mounts, used to fix sensor cubes to PMHS osseous structures, were fix on each specimen.

**Table 1. Description of the 3 PMHS used in this study.**

Test #/PMHS ID	C-1/196	C-2/191	C-3/220	Average	Range
Age at Death/Gender	61/F	70/M	62/M	64	9
Weight (kg)	80.7	54.4	81.6	72.3	27.2
Post-Mortem Stature <sup>1</sup> (mm)	1727	1701	1752	1727	51
Stretched Stature <sup>2</sup> (mm)	1870	1785	1859	1838	85
Height Change <sup>3</sup> (%)	8.3%	4.9%	6.1%	6.4%	3.3%
Cause of Death	Ovarian Cancer/ Pulmonary Edema	Cardiac Arrest	Liver Cancer		

1- Height measured post-mortem with each PMHS lying supine.

2- Height measured by scaling a video image of PMHS in pre-test position.

3. Height change is a measure of how much the stature of each PMHS increased by vertically supporting the PMHS by the upper body.

Most notably mounts were installed at the head near the posterior projection of the head center of gravity (CG), on the first thoracic vertebra (T1) where the neck meets the thorax, on the eighth thoracic vertebra (T8) near the thorax CG, and on the sacrum near the pelvis CG. Mounts on the head, T1 and sacrum were used to hold one type sensor cube (44 mm x 44 mm x 31 mm, 180g), and the one at T8 was used to hold a smaller sensor cube (21 mm x 21 mm x 15 mm, 13 g).

On the head, the mount was a 52 x 52 mm piece of 3.2 mm thick aluminum plate attached with bone screws directly to the posterior skull. On T1, the mount was a “U”-shaped aluminum structure that straddled the spinous processes of the vertebral column and bolted directly to the vertebral body of the T1 vertebra. The mount at T8 was simply a deep threaded bone screw with a 20 x 20 mm 3.2 mm thick aluminum plate brazed to its head. The mount was screwed directly into the vertebral body just to the right of the spinous process. The mount on the sacrum was a 35 mm x 90 mm x 3.2 mm thick piece of aluminum screwed directly to the sacrum between the second and third sacral foramen with two bone screws.

The location of the head CG was found by first marking the Frankfurt planes on each PMHS’ head. The lateral projections of the head CG were marked at a location 8.5 mm anterior to the trignon and 25% of the vertical distance from the Frankfurt plane to the top of the head above the Frankfurt plane (Robbins, 1983). The posterior projection of the head CG was marked at a location determined by bisecting a head exterior contour that connected the two lateral projections of the head CG. If the head instrumentation mount could not be mounted at this location due to skull curvature, the head instrumentation mount was attached superior to this point. In these cases, a screw was used to mark the posterior projection of the head CG.

After preparation each specimen was returned to the refrigerator until the day of the test. On the day of the test, the specimen was removed from the

refrigerator to allow the core body temperature to equilibrate with the room temperature ( $22^{\circ}\text{C} \pm 3^{\circ}\text{C}$ ) prior to the test. At this time the sensor cubes were mounted to the specified locations using screws. The specimens were clothed in a semi-permeable TYVEK<sup>®</sup> shirt and pants interiorly, a cotton/elastic blend shirt and pants exteriorly, and a new pair of athletic shoes (Corey, Athletic Works, from Wal-Mart Stores Inc., Little Rock, AK).

A wireless data acquisition system (TDAS G5, DTS, Seal Beach, CA), used to sample the data from the instrumentation, was padded and inserted into a cylindrical dry-bag with radius 9 cm and length 32 cm (3.4 kg with the data acquisition system). The bag was attached to the PMHS posteriorly over the lumbar spine using plastic tie-wraps (see Figure 5).

### Dummy Preparation

The dummy was prepared as specified by its developers. The dummy was clothed in the standard shoes, standard shorts, and all of the flesh and jacket was positioned appropriately.

The dummy was equipped with similar external sensor cubes as used on the top of the thorax and pelvis of the PMHS. On the head however, no external instrumentation was used. Finally the instrumentation bag used in the PMHS was mounted to the dummy’s lumbar area via plastic tie-wraps.

### Support

After the dummy and PMHS were prepared, they were outfitted with harness straps to facilitate positioning for the test. In the dummy, the harness consisted of a rope that was tied through the eye bolts of the shoulders on the dummy (Figure 4). The harness for the PMHS consisted of two sections of seatbelt webbing. One longer piece (the shoulder strap) was directed under the arms of the PMHS anteriorly and across the posterior thorax. The second seatbelt strap

was split longitudinally in the middle so that half of the strap could be positioned under the PMHS chin and the other half could slip under the occiput (Figure 4).

At this time, the surrogate was hoisted into position over the pedestrian sled. The harness was then transferred to the release hardware. It should be noted that the lengths of the two harness straps used in the PMHS tests were such that the majority of the weight of the PMHS was being supported by the shoulder strap. The head strap is only used to orient the head in a neutral position prior to the test.

The release hardware consisted of a plate rigidly mounted to the laboratory roof, with a threaded rod going through the plate. At the end of the threaded rod, a tension load cell was attached to determine the timing of surrogate release (Figure 4). A solenoid release mechanism, mounted below the load cell, was used to release the support harness just prior to vehicle impact.

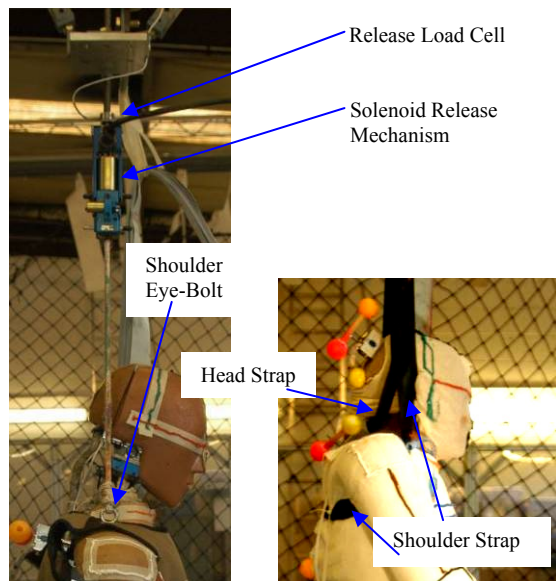


**Figure 4. Support methods for both the dummy (left) and PMHS(right). Note that the shoulder strap used with the PMHS (right) mostly obscures the head strap. Only half of the split strap can be seen as it passes under occiput of the PMHS.**

### Positioning

Data from the pedestrian crash data study (PCDS) suggest that the majority of pedestrians are struck laterally with their lower extremities positioned in a gait-like position (Kam *et al.* 2005). Thus, all surrogates in this study were positioned laterally at the vehicle center line in a mid-stance gait position (Figure 5). Since arm position can potentially affect upper body kinematics to a level that would reduce the severity of thoracic and head loading (Kam *et al.* 2005), the arms were bound at the wrists anterior to the

surrogate. The right wrist was placed farthest from the body and the left wrist was placed closest to the body when the wrists were bound. This positions the struck-side elbow slightly anterior to the thorax and thus reduces the potential for the arm to affect the upper body kinematics (Kam *et al.* 2005).

The height of the dummy, as measured after positioning in each test, varied between 173 cm and 174 cm. The standing height of each PMHS after positioning is given in Table 1 as the “stretched stature”.

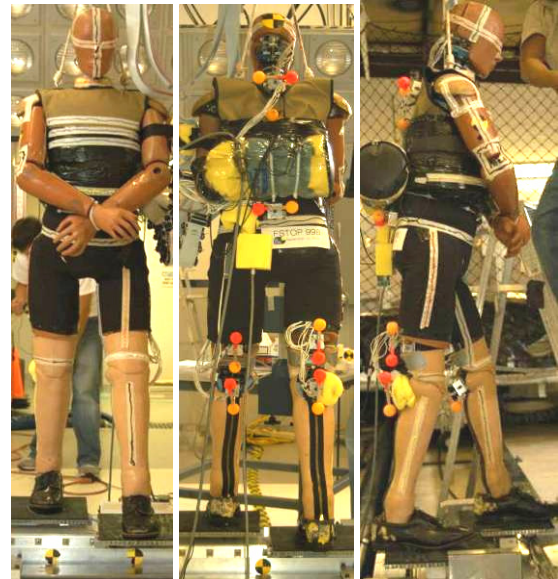


**Figure 5a. Typical position of the dummy prior to each test.**



**Figure 5b. Typical position of the PMHS immediately prior to each test.**

## Test Event

After positioning of the surrogate was complete, the vehicle sled was propelled down the tracks toward the pedestrian. The vehicle sled passed an inductive sensor on the track that triggered the release of the surrogate between 19 and 26 ms before initial bumper contact (Table 2). The vehicle speed was recorded using a similar sensor, and was approximately 40 km/h in each test (Table 2).

After the vehicle struck the pedestrian surrogate, then impacted and accelerated the pedestrian sled, and approximately 200 ms later, both sleds contacted the decelerator. This caused the vehicle to decelerate, and pedestrian surrogate to be lofted forward into the catching mechanism. After the test the wrap around distance (WAD) to head strike was measured (Table 2).

## KINEMATICS MEASUREMENT

Analysis of pedestrian surrogate kinematics during the impact event were performed using high speed video images taken from an off-board camera on the driver's side of the vehicle during all of the tests. The camera used to capture the high speed video (Phantom V5.0, Vision Research, Wayne, NJ) sampled 1024 pixel by 1024 pixel (1.0 mega pixel) images at 1000 Hz during all of the tests.

The camera's field of view stretched 3.78 m horizontally from approximately 30 cm up the tracks from the positioned surrogate to about 60 cm down past the tip of the decelerator push rod. The field of view of the imager was sufficient to permit motion tracking of all points on each surrogate and the vehicle from 40 ms prior to initial contact, to the time that the vehicle began to decelerate. High speed video images (at 20 ms intervals) from a representative dummy and PMHS test are given in Figure 6.

**Table 2. Vehicle velocity, surrogate release time and wrap around distance (WAD) to head strike for all six tests.**

	Test #	Vehicle Velocity km/h	Release Time <sup>1</sup> ms	Head Strike (WAD) mm
Dummy	D-1	39.69	-19.6	1930
	D-2	40.02	-26.3	1940
	D-3	39.88	-21.6	1970
PMHS	C-1	39.75	-20.2	2410
	C-2	39.56	-25.6	2200
	C-3	39.88	-24.7	2320

1-Time zero is defined as the initial contact between the vehicle's bumper and the surrogate's lower extremity

## Photo Targets

Since no external instrumentation mount was used on the dummy's head, a quadrant type photo target was mounted on the dummy's head at the posterior projection of the CG for all tests (as determined by the drawing of the head).

Most of the other photo targets used were dumbbell-type targets consisting of two 38 mm diameter table tennis balls, painted in contrasting colors, mounted at both ends of a wooden rod (63.5 mm in length). Each photo target was fixed to the outer surface of each sensor cube with a piece of threaded rod. The dumbbell photo targets were positioned so that the center of the wooden rod was directly over the center of the sensor cube (and thus directly over the center of the mount location) and approximately 38 mm from the sensor cube's outer face (Figure 7).

Dumbbell-type photo targets were mounted to the sensor cubes on the dummy near the pelvis CG, and at the top of the thorax (T1). On the PMHS, dumbbell-type photo targets were mounted to sensor cubes at the head, T1, and pelvis.

A single 38 mm table tennis ball was used as a photo target at the thorax CG for both the Polar-II and PMHS. In the Polar-II, a specially designed mount was installed near the CG of the thorax that permitted the ball (attached to a plastic tube) to be positioned directly over the posterior projection of the thorax CG point (Figure 7). For the PMHS, duct tape was added over the sensor cube and the ball was attached to the duct tape with foam tape.

Whenever possible the sensor cube mounted on the PMHS head was mounted at the posterior projection of the head CG (permitting the dumbbell type photo target mounted to the cube to be used to track head motion). However, when the instrumentation mount had to be mounted superior to this point, table tennis ball was screwed directly to the PMHS skull at the posterior projection of the CG point. In all cases, all of the targets were rigidly secured to either the steel structure of the dummy or osseous structures in the PMHS.

## Phototarget Tracking

The motion of all of the photo targets (head CG projection, T1 or top of thorax, T8 or thorax CG projection and pelvis CG projection for both the dummy and the PMHS) were tracked throughout the impact event (Figure 8). In all cases that the motion of a dumbbell type photo target was measured, the motions of both target balls were measured.

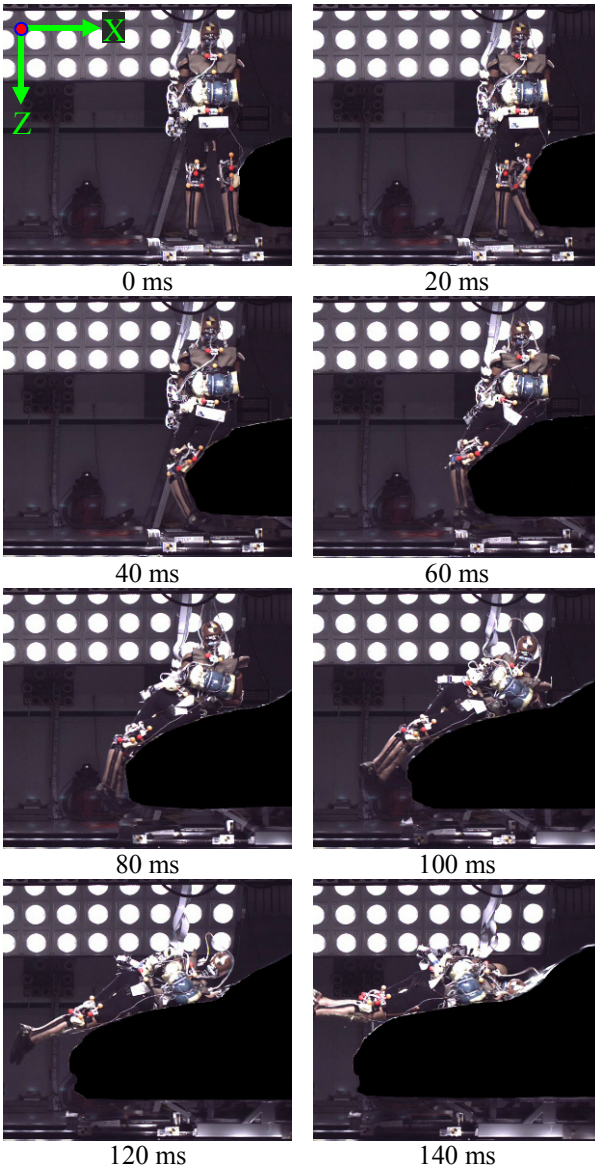


**Figure 6a. High speed video images of a typical dummy test.**

The motion of each photo target was measured by recording the location, in pixels, of each photo target from high speed video images that were re-sampled at 250 Hz. The time of initial contact between the vehicle bumper and the surrogate's lower extremity was defined to be  $t=0$ . The first video analysis frame was 40 ms prior to  $t=0$ , at  $t=-40$  ms.

The time of head strike was determined to mark the end of the time interval of interest for computing kinematic trajectory data. In each test the time of head strike was determined by visual examination of the video data. Since the trajectory data are only sampled at 250 Hz, the time of head strike was then rounded to the nearest 4 ms so that it corresponded with an analysis frame (Table 3). To facilitate accurate head

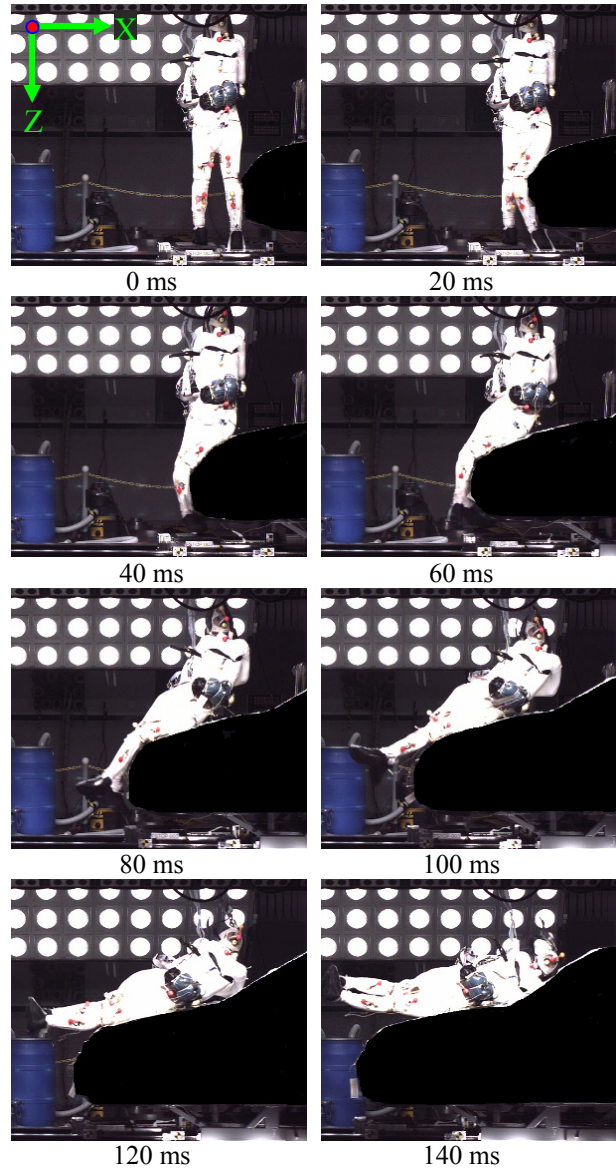


**Figure 6b. High speed video images of a typical PMHS test**

velocity measurement during head strike, the last video frame that was digitized was the frame 20 ms after the head-strike frame (Table 3).

### Data Analysis

For the discussion of the methodology used to analyze the trajectory data, two coordinate systems must be defined. The frame coordinate system, defined by the view of the high speed imager, is fixed with respect to the laboratory. The  $x$  and  $z$  directions are defined as the horizontal and vertical axes of the imager frame, respectively. Positive  $x$  is to the right (the vehicle travels in the negative  $x$  direction) and positive  $z$  points down. The motions of all of the photo

targets were tracked in the frame coordinate system. The second coordinate system, the vehicle coordinate system, will be defined later.

To obtain the motion of the center of the dumbbell-type targets, the  $x$  and  $z$  coordinates (in the frame coordinate system) of each ball on the target were averaged at each sampled frame. Then all of the parametric trajectory signals (each target had  $x(t)$  and  $z(t)$  signals) were de-biased so that each signal's value was 0 pixels at the first time step (-40 ms).

Then each of the trajectory signals was converted to a measurement in mm by multiplying each signal by 3.695 mm/pixel and each vehicle signal by 3.243 mm/pixel. These values for the spatial resolution of the imager at the surrogate plane and at the driver's-side vehicle exterior plane (where the motion of the vehicle was tracked) were determined prior to the test. The absence of significant edge effects was determined because a maximum difference in spatial resolution of only 0.2 mm/pixel was measured at the edges of the camera's field of view.

The filtering convention specified in ISO/DIS 13432-4 (ISO, 2004) was adopted to smooth the position data. All signals were filtered with four passes of the moving average filter given in Equation 1.

$$\begin{aligned} x_{i,f} &= \frac{x_{i-1,fcs} + 2x_{i,fcs} + x_{i+1,fcs}}{4} \\ z_{i,f} &= \frac{z_{i-1,fcs} + 2z_{i,fcs} + z_{i+1,fcs}}{4} \end{aligned} \quad (1).$$

In Equation 1,

- $x_{i,f}$  and  $z_{i,f}$  are the filtered  $x$  and  $z$  positions, in the frame coordinate system, at frame  $i$ , in mm, and
- $x_{i,fcs}$  and  $z_{i,fcs}$  are the unfiltered (or filtered on the previous pass)  $x$  and  $z$  positions, in the frame coordinate system at frame  $i$ , in mm.

The second coordinate system important to this analysis is the vehicle coordinate system. The vehicle coordinate system is defined to be fixed with respect to the vehicle's motion. The origin is defined by the  $x$  coordinate of the head CG photo target at the analysis frame taken at time  $t=0$  ms, and by the  $z$  coordinate of the simulated ground level (the level of the platforms on the pedestrian sled) (Figure 9). In the vehicle coordinate system the positive  $z$  direction points down and the frame coordinate system (fixed with respect to the lab) moves in the positive  $x$  direction. It is important to note that the location of the origin in the  $x$  direction is defined separately in each individual test,

while the location of the origin in the  $z$  direction remains constant from test to test.

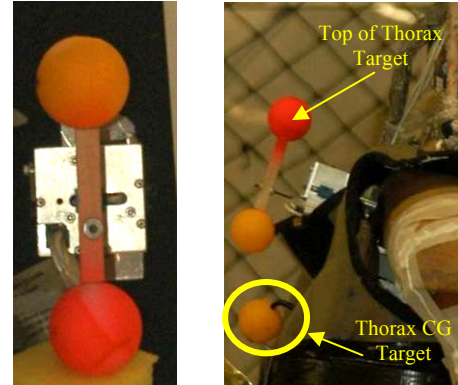


**Figure 7. Dumbbell-type photo targets.** At left, a dumbbell-type photo target is shown. The image on the right shows how a dumbbell-type photo target was mounted to the sensor cube at the T1 location in the dummy. The single-ball photo target used to track the thorax CG of the dummy is also shown.

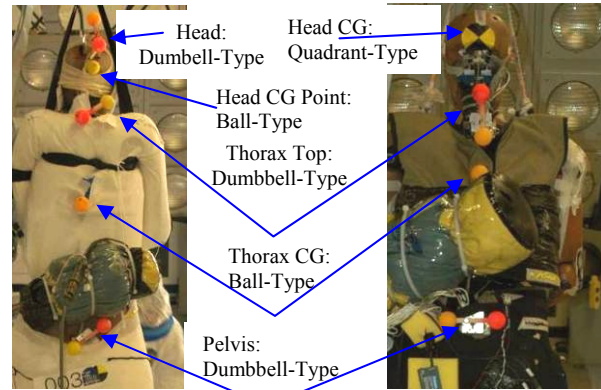


**Figure 8. Photo targets used in the dummy (top) and PMHS (bottom) tests.** Note these images are not at the same scale.

**Table 3. Test type, time of head strike, digitized frame closest to the time of head strike and last frame digitized for each test in the study.**

	Test	Time of Head Strike (ms)	Head Strike Imager Frame	Last Frame Analyzed
Dummy	D-1	126	128	148
	D-2	126	128	148
	D-3	131	132	152
PMHS	C-1	152	152	172
	C-2	138	136	156
	C-3	144	144	164

To compute the trajectory signals in the vehicle coordinate system, the motion of each target had to be subtracted from the vehicle motion and the origin of each signal had to be shifted in space to its origin as defined by the vehicle coordinate system.

The distances between each body segment's photo target (and the origin of its trajectory) and the origin of the vehicle coordinate system in the  $x$  and  $z$  directions,  $s_x$  and  $s_z$ , were measured in pixels and converted to mm using the frame taken at  $t=0$ .

Equation 2 explains how frame coordinate system parametric trajectory signals were transferred to the vehicle coordinate system by subtracting the vehicle's motion and shifting the trajectory origin.

$$\begin{aligned} x_i &= s_x + (x_{i,f} - v_{x,i,f}) - (x_{0,f} - v_{x,0,f}) \\ z_i &= s_z - (z_{i,f} - v_{z,i,f}) + (z_{0,f} - v_{z,0,f}) \end{aligned} \quad (2).$$

In Equation 2,

- $x_i, z_i$  are the  $x$  and  $z$  coordinates, of each body segment's trajectory, in the vehicle coordinate system, at frame  $i$ , in mm,
- $v_{x,i,f}, v_{z,i,f}$  are the filtered  $x$  and  $z$  positions of the vehicle photo target at frame  $i$ , in mm,
- $x_{0,f}, z_{0,f}$  are the filtered  $x$  and  $z$  positions of each of the surrogate photo targets at frame zero (corresponding to time  $t=0$ ), in mm, and
- $v_{x,0,f}, v_{z,0,f}$  are the filtered  $x$  and  $z$  positions of the vehicle photo target at frame zero (corresponding to time  $t=0$ ), in mm.

The velocity of the head was calculated by adopting the methodology used in ISO/DIS 13232-5 (ISO, 2004) and given in Equation 3.

$$\begin{aligned} V_{x,i} &= \frac{x_{i+1} - x_{i-1}}{t_{i+1} - t_{i-1}} \\ V_{z,i} &= \frac{z_{i+1} - z_{i-1}}{t_{i+1} - t_{i-1}} \end{aligned} \quad (3).$$

In Equation 3,

- $V_{x,i}, V_{z,i}$  are the head photo target's velocity, in m/s, in the  $x$  and  $z$  directions at frame  $i$ , and
- $t_i$  is the time, in ms, at frame  $i$ .

The resultant of the velocity signal is then computed by calculating the magnitude of the velocity vector defined by the parametric components in Equation 3 at each time step.



**Figure 9. Vehicle coordinate system. The green cross represents the vehicle coordinate system origin.**

## PMHS KINEMATICS

Trajectory data for the head CG, T1, T8 and the pelvis are given in the vehicle coordinate system (Equation 2) for the PMHS tests in Figure 10. In each of the three plots given in Figure 10, the vehicle center line contour is added for reference. To provide an indication of the time scale, lines connecting each segment's trajectory at 12 ms intervals are also included. In each test, the trajectory signal is plotted from time  $t=0$  to the time of head strike (also given in Table 3). Time histories of head resultant velocity from each of the PMHS tests are given in Figure 11.

## KINEMATIC TRAJECTORY CORRIDORS

### Scaling Kinematics Data

To provide a basis for comparing surrogate kinematics, it is common to scale PMHS response using a length scale factor. A scale factor is used to scale the geometry of the PMHS to a reference geometry. Since one goal of this study is to compare the kinematic response of the PMHS and the dummy, the dummy geometry was chosen as the standard, or reference geometry, to use in scaling the PMHS kinematics data.

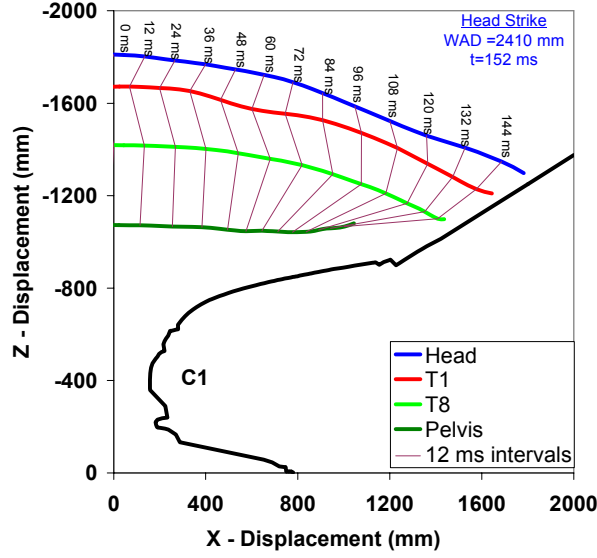


Figure 10a. Vehicle coordinate system trajectories for test C-1. The vehicle center line contour is in black. Purple lines, labeled “12 ms intervals”, connect body segments at each specified time.

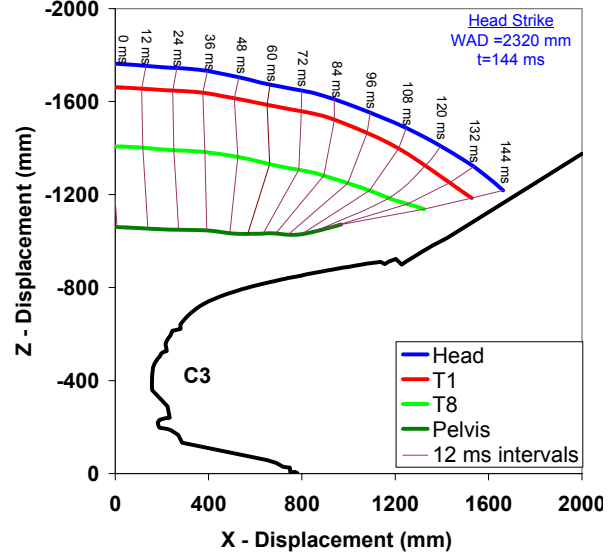


Figure 10c. Vehicle coordinate system trajectories for test C-3.

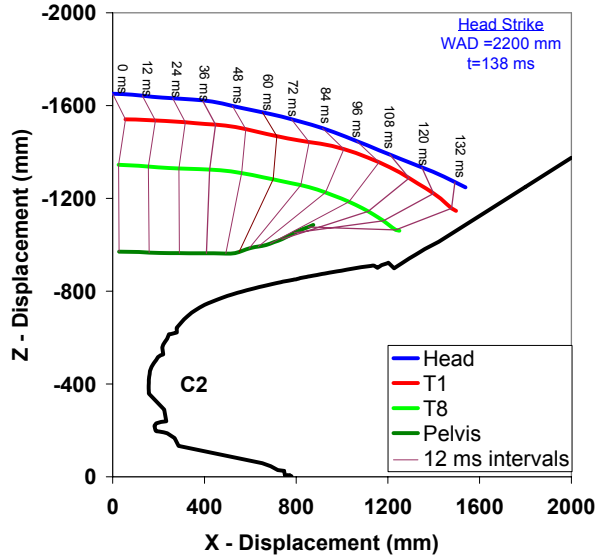


Figure 10b. Vehicle coordinate system trajectories for test C-2.

Recognizing that PMHS body-segment lengths vary slightly from PMHS to PMHS, and the lengths of the Polar-II body segments are also slightly different than those of the PMHS (Table 4), it was determined that individual scale factors should be used to scale trajectory data from each body region. Thus twelve individual scale factors were calculated to account for the head CG, T1, T8 and pelvis trajectories for all three PMHS tested. None of the dummy trajectory data were scaled.

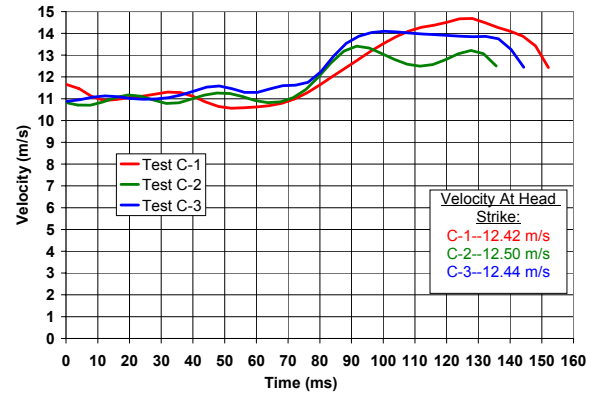


Figure 11. Head resultant velocity from the PMHS tests. Note that each signal is plotted from  $t=0$  until the time of head strike for each particular test.

The distances between each body segment’s photo target and the origin of vehicle coordinate system in the  $z$  direction,  $s_{z,s}$ , were averaged for all of the dummy tests (Table 4). Using the average values,  $s_{z,d}$ , and the same measurements, from the PMHS tests,  $s_{z,c}$ , twelve scale factors were developed to scale each of the four trajectories in each test (Table 4). An example calculation to obtain the T8 scale factor in test 002,  $\lambda_{002,T8}$ , is given in Equation 4.

$$\lambda^{T8,C-2} = \frac{s_{z,d}^{T8}}{s_{z,c}^{T8,C-2}} = 1.0027 \quad (4).$$

**Table 4. Initial vertical distance of each body segment's photo target and PMHS scale factors. Only summary data of dummy target heights are provided due to their similarity. Vertical distances appear as negative numbers because positive z is defined in the downward direction. All values are in mm.**

	Photo Target Initial Height From Ground Level							Height Scale Factors				
	Dummy Mean	Dummy Range	Test C-1	Test C-2	Test C-3	PMHS Mean	PMHS Range	Test C-1	Test C-2	Test C-3	Mean	Range
Head CG	-1705	4	-1811	-1652	-1763	-1742	159	0.9415	1.0321	0.9672	0.9802	0.091
Top of Thorax	-1479	13	-1670	-1541	-1663	-1625	129	0.8853	0.9596	0.8893	0.9114	0.074
Thorax CG	-1349	15	-1419	-1345	-1408	-1391	74	0.9505	1.0027	0.9580	0.9704	0.052
Pelvis CG	-1042	11	-1073	-970	-1060	-1035	103	0.9707	1.0743	0.9826	1.0092	0.104

-All measurements are in mm.

In Equation 4,

- $S_{z,d}^{T8}$  is the average of the  $s_z$  values for the thorax CG from the three dummy tests, in mm, and
- $S_{z,c}^{T8,C-2}$  is the  $s_z$  value, in mm, for T8 in test C-2.

The filtered surrogate trajectory data,  $x_{i,f}$  and  $z_{i,f}$ , (Equation 1) were then multiplied by their respective scale factors to obtain the scaled frame coordinate system trajectories  $x_{i,f}^*$  and  $z_{i,f}^*$ . It is important to note that all scaled values are indicated in this study with an asterisk.

The scaled trajectories,  $x_{i,f}^*$  and  $z_{i,f}^*$ , were then converted to the vehicle coordinate system (to obtain  $x_i^*$  and  $z_i^*$ ) using Equation 5.

$$\begin{aligned} x_i^* &= s_x \lambda_L + (x_{i,f}^* - v_{x,i,f}^*) - (x_{0,f}^* - v_{x,0,f}^*) \\ z_i^* &= s_z \lambda_L - (z_{i,f}^* - v_{z,i,f}^*) + (z_{0,f}^* - v_{z,0,f}^*) \end{aligned} \quad (5).$$

Since the trajectory of each body region is defined with two parametric trajectory signals,  $x(t)$  and  $z(t)$ , if the positions (dependant variable) are scaled, time (independent variable) must be scaled as well. Since a different scale factor is used to scale the positions of each body region, a different scaled time at frame  $i$ ,  $t_i^*$ , had to be calculated for each body region and each test. When using a length scale factor, as in this case, time scales the same as length, so  $t_i$  was multiplied by each of the scale factors to obtain each of the  $t_i^*$  signals.

Scaled head velocities are calculated using both scaled position data and scaled time data by again employing the ISO methodology (ISO, 2004) (Equation 6).

$$\begin{aligned} V_{x,i}^* &= \frac{x_{i+1}^* - x_{i-1}^*}{t_{i+1}^* - t_{i-1}^*} \\ V_{z,i}^* &= \frac{z_{i+1}^* - z_{i-1}^*}{t_{i+1}^* - t_{i-1}^*} \end{aligned} \quad (6).$$

In Equation 6,

- $V_{x,i}^*$  and  $V_{z,i}^*$  are each photo target's scaled component velocity, in m/s, in the  $x$  and  $z$  directions at frame  $i$ .

The resultant of the scaled head velocity is computed by computing the magnitude of the scaled velocity vector defined by the parametric components in Equation 6.

## Corridor Development

**Average Curves** Since this study was only concerned with examining the trajectory data from initial bumper contact ( $t=0$ ) to head strike, and the time data were scaled, the time of head strike had to be scaled as well. Given that the time of head strike had already been rounded to the nearest analysis frame, the time of the head strike frame was scaled. Finally, the scaled time at head strike,  $t_{hs}^*$ , is rounded to the nearest analysis frame (Table 5).

When each time signal was scaled, the sampling frequency changed from 250 Hz, to the inverse of the scale factor,  $\lambda^{-1}$ , multiplied by 250 Hz. Since one scale factor was developed for each body region in each test, each scaled time signal had a different sampling frequency. To facilitate averaging and corridor development, all of the scaled trajectory and velocity data were re-sampled, by interpolation at 250 Hz, the frame at  $t=0$  to  $t=t_{hs,c}^*$ , where  $t_{hs,c}^*$  is the lowest time,  $t_{hs}^*$ , for each body region (Table 5).

**Table 5. Un-scaled and scaled head strike frame times for each body segment trajectory in each PMHS test. The earliest scaled time at head strike for each body region is also given. All times are in ms.**

	Scaled Head Strike Frame Time $t_{hs}^*$			$t_{hs,c}^*$
	001	002	003	
Un-scaled	152	136	144	-
Head	144	140	140	140
T1	136	132	128	128
T8	144	136	140	136
Pelvis	148	144	140	140

-All times are given in ms.

The average scaled PMHS trajectory was computed by averaging values of each trajectory signal at each 4 ms time interval. Averaged scaled trajectories were computed for the head, T1, T8 and pelvis. The resultant head velocities from each test were also averaged to create an average scaled resultant velocity.

Each body segment average trajectory was fit to a third order polynomial with parameters  $\alpha$ ,  $\beta$ ,  $\gamma$ , and  $\delta$  (Table 6 and Equation 7).

$$\overline{z_i^*} = \alpha \overline{x_i^*}^3 + \beta \overline{x_i^*}^2 + \gamma \overline{x_i^*} + \delta \quad (7).$$

In Equation 7,

- $\overline{x_i^*}$ , and  $\overline{z_i^*}$ , are the average scaled  $x$  and  $z$  components of each body segment's trajectory, in mm.

**Table 6. Third-order polynomial parameters for each average scaled PMHS body segment trajectory.**

	Head	T1	T8	Pelvis
$\alpha$	-1.11461E-08	9.11329E-08	6.64334E-08	-3.63583E-07
$\beta$	1.88378E-04	-1.67628E-05	5.95507E-05	3.51434E-04
$\gamma$	1.89965E-03	7.69504E-02	1.86501E-02	-5.59884E-02
$\delta$	-1.70050E+03	-1.48419E+03	-1.34781E+03	-1.03857E+03
$R^2$	0.9997	0.9930	0.9997	0.9765

The average scaled resultant head velocity curve has too complex curvature to be accurately modeled by a third (or higher) order polynomial. Thus the average and standard deviation data were re-sampled with the minimum number of points necessary to model the complexity of the signal's curvature (Table 7). Average scaled head velocity data are given from  $t=0$  to  $t=t_{hs,c}^*$ , where  $t_{hs,c}^*$  is the lowest time,  $t_{hs}^*$  for the

head (Table 5). The standard deviation data given in Table 7 are calculated by taking the square root of the bias-corrected variance (this contains the “n-1” correction term in the denominator of the definition).

**Corridors** Typically response corridors based on PMHS data are developed by incorporating the standard deviation of the data into the calculation of the upper and lower corridor bounds (Lessley *et al.* 2004, Viano and Davidsson 2002, and Maltese *et al.* 2002). However, due to similarity between the PMHS trajectories (after scaling) and the number of data sets (only 3), boxed-standard deviation corridors for PMHS body segment trajectories were determined to be too narrow for dummy or computational model development or validation. Even standard deviation corridors with a two-standard deviation width were too narrow (Figure 12).

**Table 7. Tabulated average and standard deviation of the scaled average PMHS head velocity signal.**

Time ms	Head Velocity m/s	Standard Deviation m/s	Time ms	Head Velocity m/s	Standard Deviation m/s
0	11.34	0.931	77	11.97	0.825
7	11.20	0.766	84	12.95	0.863
14	11.24	0.556	91	13.67	0.729
21	11.33	0.491	98	13.96	0.829
28	11.30	0.664	105	13.93	1.162
35	11.29	0.745	112	13.85	1.441
42	11.36	0.595	119	13.93	1.516
49	11.34	0.492	126	13.94	1.200
56	11.23	0.416	133	13.84	0.903
63	11.27	0.638	140	12.91	0.869
		70   11.44   0.753			

Because kinematic corridors based on the standard deviation of the data are too narrow, corridors needed to be developed for PMHS body segment trajectories using a different methodology. The corridors would ideally begin very narrow (because the scaling procedure forces the origin of all trajectories for each body segment to the same point), and gradually grow wider to account for variability in the data as the length of the trajectory grows.

Thus, kinematic response corridors were calculated for the head, T1, T8 and pelvis trajectories using the average trajectories and the path length of each trajectory (Equation 8).

$$S_i = \sum_{j=1}^i \sqrt{\left(\overline{x_j^*} - \overline{x_{j-1}^*}\right)^2 + \left(\overline{z_j^*} - \overline{z_{j-1}^*}\right)^2} \quad (8).$$

In Equation 8,

- $S_i$  is the total path length of the trajectory measured up to frame  $i$ , in mm.

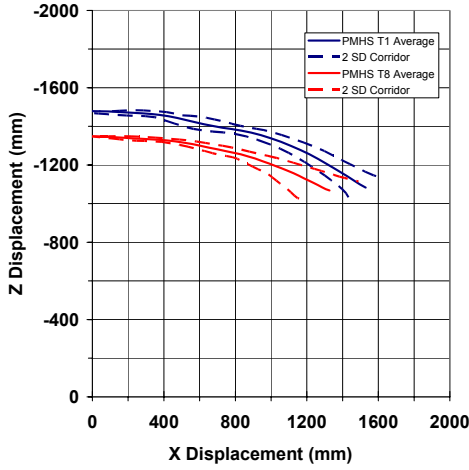


**Figure 12. Averaged scaled T1 and T8 trajectory data with boxed-standard deviation corridors using a two-standard deviation width.**

Boxed corridors were then developed using the path length. Boxed-corridors can be developed by creating a square around each data point in the curve, with edges aligned with the coordinate axes, where the length of the square is equal to  $2k$ . For the current study,  $k$  is some percentage of the trajectory's path length. Two pairs of parametric trajectory signals were calculated to determine the path of the corner's of the path length square. The four signals were calculated using Equation 9.

$$\begin{aligned} C_{x,i}^+ &= x_i^* + kS_i \\ C_{x,i}^- &= x_i^* - kS_i \\ C_{z,i}^+ &= z_i^* + kS_i \\ C_{z,i}^- &= z_i^* - kS_i \end{aligned} \quad (9).$$

In Equation 9,  $C_{x,i}^+$  gives the  $x$  component of the signal formed by adding the  $x$  component of the average parametric body segment trajectory at frame  $i$  to  $k$  percent of the path length at frame  $i$ .  $C_{x,i}^-$ ,  $C_{z,i}^+$ ,

$C_{z,i}^-$  provide similar signals. It is important to note that the values calculated using Equation 8 and Equation 9 are calculated using the values of the trajectories obtained from the third order polynomial equations (Equation 7) defined by the parameters in Table 6.

By combining the  $x$  and  $z$  components of the two pairs of parametric trajectory signals in Equation 9, the trajectory of each path length square's corners can be plotted. Since the path length square is aligned with respect to the coordinate frame and the trajectory signals show more  $x$  direction displacement than  $z$  direction displacement, the trajectory of two of the path length square's corners will be above the average body segment trajectory and two of the corners' trajectories will be below the average trajectory. The upper bound for each body-segment corridor was chosen to be the trajectory of the path length square's corner that remained farthest above the average curve for the longest time. The lower bound was chosen to be the trajectory of the path length square's corner that remained farthest below the average curve for the longest time. Due to the downward concavity of the average trajectory signals (with  $+z$  pointing down), the kinematic response corridors for the head CG, T1 (or top of thorax) and T8 (or thorax CG) trajectories were developed by plotting  $C_{x,i}^+$  vs.  $C_{z,i}^-$  (for the upper bound) and  $C_{x,i}^-$  vs.  $C_{z,i}^+$  (for the lower bound). Since the pelvis average scaled trajectory is concave upward, the upper bound of the pelvis corridor was developed by plotting  $C_{x,i}^+$  vs.  $C_{z,i}^+$ , and the lower bound was developed by plotting  $C_{x,i}^-$  vs.  $C_{z,i}^-$ . Any value of  $k$  can be used to develop corridors of varying width for each body segment's trajectory. Figure 13 presents each of the scaled average body segment trajectories (fit to third order polynomials) plotted with three sets of corridors for  $k=4\%$ ,  $k=8\%$  and  $k=12\%$ .

Kinematic response corridors (Figure 14) were also developed for scaled head velocity by incorporating the standard deviation (Table 7) because it did not create a corridor that was too narrow for dummy validation. The corridor boundaries for the head velocity corridor are determined by adding  $m$  standard deviations to (upper bound), or subtracting  $m$  standard deviations from (lower bound), the average scaled PMHS head resultant velocity at each time step. Figure 14 provides the averaged scaled PMHS head resultant velocity curve and corridor boundaries for  $m=0.5$ ,  $m=1.0$  and  $m=1.5$  standard deviation corridors.

## DISCUSSION

The trajectory analysis discussed in the "Data Manipulation" portion of the "Kinematics Measurement" section was performed for both the PMHS tests and the dummy tests. Dummy trajectory signals, as calculated in Equation 2 and Equation 3, provide evidence that the Polar-II can produce a repeatable response in a full-scale pedestrian impact

tests (Figures 15 and 16). Plotting the average PMHS trajectory signal with the dummy signals provides a basis for comparison of the dummy body segment trajectories and PMHS body segment trajectories (Figure 15). The Polar-II was shown to generally fall within 10% path length corridors, so the 10% path length corridors are included in Figure 15.

In comparison of dummy and PMHS trajectories, one interesting feature is that PMHS trajectories and dummy trajectories are not the same length. Despite the scaling procedure, PMHS trajectories are still significantly longer, typically in the  $x$ -direction, than dummy trajectories. This is also evident in that head strike in the PMHS tests typically occurred at a much larger WAD (2410, 2200 and 2320 mm) than in the dummy tests (1970, 1980 and 1990 mm). Additionally, the time of head strike in the PMHS tests is, on average, greater than the time of head strike in the dummy tests (Table 3). These results suggest that PMHS specimens traversed longer distances in the  $+x$  direction than the dummy did between initial vehicle contact and head strike. Further examination of the video data suggests that this is, at least partially, due to the fact that the PMHS slides farther up the hood than the dummy does prior to head strike.

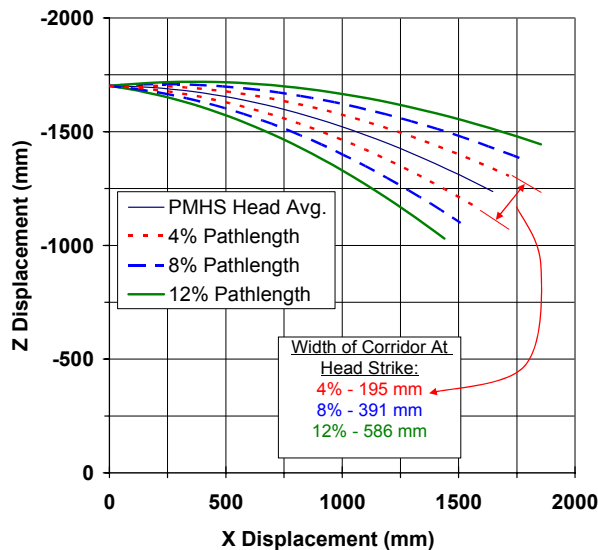


**Figure 13a. Scaled average PMHS head trajectory (from the third order polynomial with parameters given in Table 6) with 4%, 8% and 12% path length corridors and corridor width at head strike.**

Two factors seem to influence the amount of sliding that occurs in each surrogate. Firstly, it was noted that there was a significantly different damage pattern on the hood leading edge of the vehicle after a dummy test than after a PMHS test. Sliding up the hood by pedestrian surrogates is promoted by the smooth sloping shape of the hood. One potential

explanation for less sliding with the dummy is that either the mass, mass distribution, or stiffness of the dummy thigh and/or pelvis are not totally biofidelic. Thus a different damage pattern could be caused to the lower edge of the hood, changing its smooth shape, and restricting sliding. Secondly, the PMHS and the dummy wore different clothing during the tests. It is further hypothesized that differences in the frictional characteristics of the standard dummy shorts, and the cotton/elastic pants worn by the PMHS.

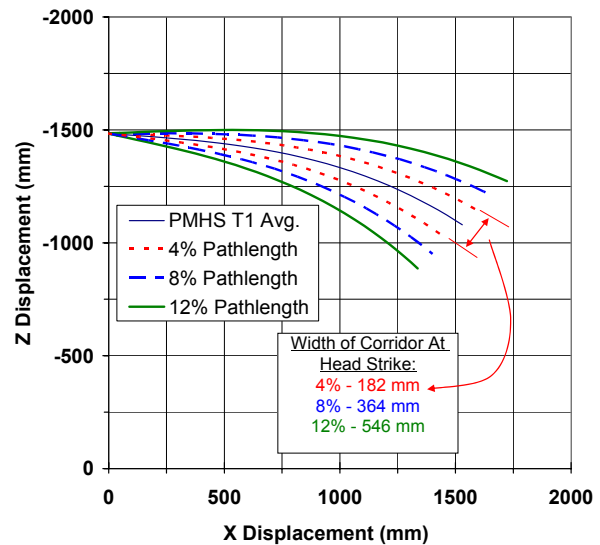


**Figure 13b. Scaled average PMHS T1 trajectory (from the third order polynomial with parameters given in Table 6) with 4%, 8% and 12% path length corridors and corridor width at head strike.**

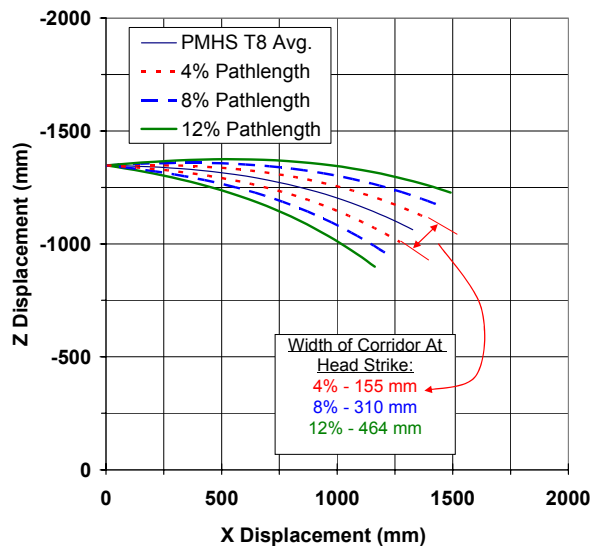


**Figure 13c. Scaled average PMHS T8 trajectory (from the third order polynomial with parameters given in Table 6) with 4%, 8% and 12% path length corridors and corridor width at head strike.**

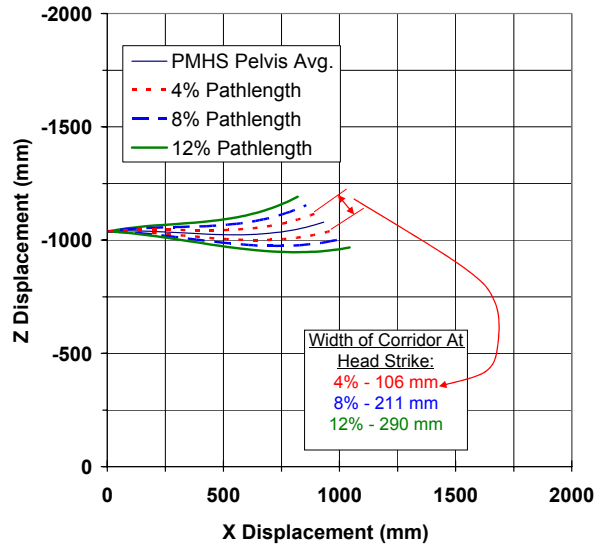


**Figure 13d. Scaled average PMHS pelvis trajectory (from the third order polynomial with parameters given in Table 6) with 4%, 8% and 12% path length corridors and corridor width at head strike.**

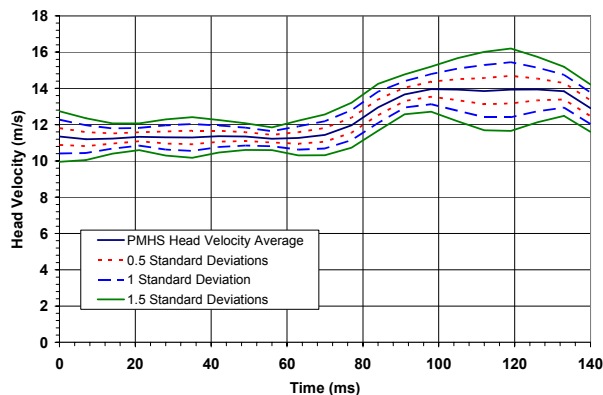


**Figure 14. Scaled average PMHS head resultant velocity time history with 0.5, 1.0 and 1.5 standard deviation corridors.**

Greater sliding in the PMHS tests causes increased length of the body segment trajectories, later head strike times, and longer WADs to head strike than in the dummy tests. More testing is necessary to determine the all of the factors that contribute to sliding.

An additional reason for differences in trajectory length and WAD to head strike is that is that the PMHS head starts farther from the ground level at  $t=0$  than the dummy. Although the statures of the PMHS, as measured post-mortem, were between 170 cm and 175 cm, when the PMHS were hoisted over the pedestrian sled and positioned, their heights had increased to 178 cm to 187 cm. The dummy's pre-test stature measured

only 173-174 cm. The change in PMHS stature due to supporting the PMHS by the upper body (5% to 8%) is due to stretching of the spine under the tension caused by the PMHS weight.

It was impossible to support any significant portion of the PMHS weight by the PMHS lower extremities. Lowering the release mechanism only caused an increase in flexion at the knee and hip joints in the PMHS, rather than increasing the load supported by the lower extremities. Artificially stiffening the knee and hip joints of the PMHS could have permitted a small amount of the upper body weight to be supported by the lower extremities. However, artificial joint stiffening was not performed because it was determined that any joint stiffening would ultimately affect the joint stiffness and range of motion. Thus, no adjustment for the stretched stature of the PMHS could be made by attempting to get the PMHS to support its own weight.

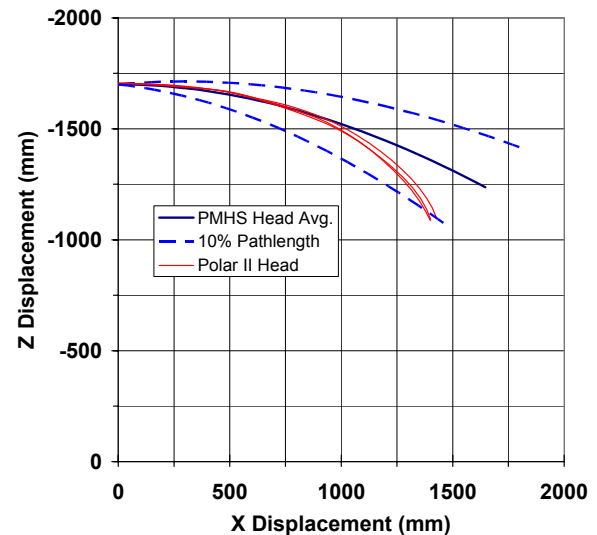


**Figure 15a. Dummy head trajectories with the average scaled PMHS head trajectory and 10% path length corridors.**

Since it was not possible to get the PMHS lower extremities to support any of the upper body weight, some differences in pre-test position between the dummy and the PMHS arose (Figure 5). Most notably, not as much anterior-posterior separation between the knee joints was possible in the PMHS tests as used in the dummy tests. Another difference in position between the dummy and the PMHS can be seen in the angle the dummy's spine makes with respect to the ground (lateral picture, Figure 5a). The angle of the spine in the dummy tests was produced as a result of a limited range of motion of the dummy hip in extension. The range of motion was limited due to the orientation

of the hip and pelvis flesh (without the flesh the range of motion is greater). The limited range of motion required the dummy pelvis to be pushed posteriorly so that the dummy's feet could be placed on the pedestrian sled foot plates. This alignment produces a forward-tilt in the spine.

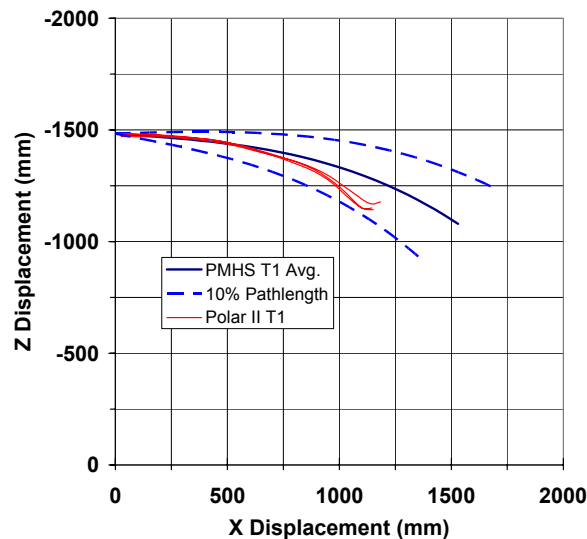


**Figure 15b. Dummy top of thorax (T1) trajectories with the average scaled PMHS T1 trajectory and 10% path length corridors.**

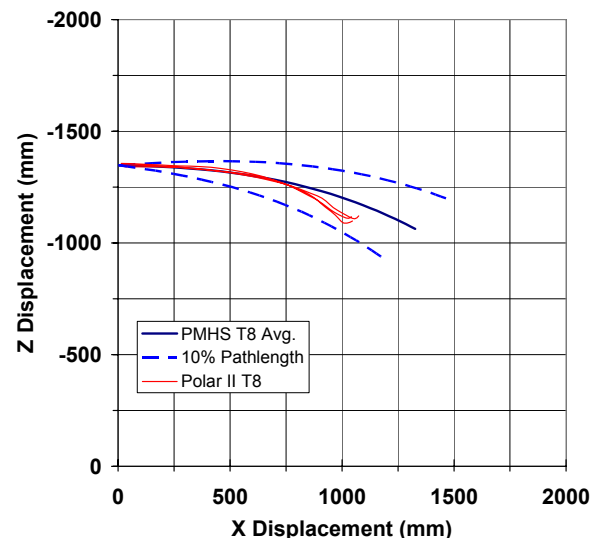


**Figure 15c. Dummy thorax CG (T8) trajectories with the average scaled PMHS T8 trajectory and 10% path length corridors.**

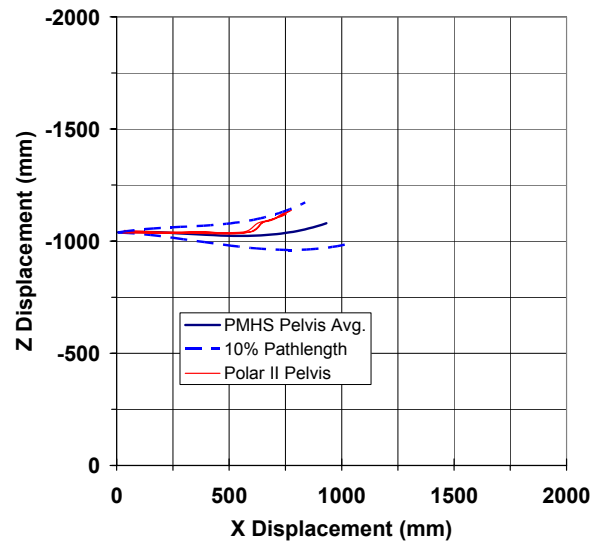


**Figure 15d. Dummy pelvis trajectories with the average scaled PMHS pelvis trajectory and 10% path length corridors.**

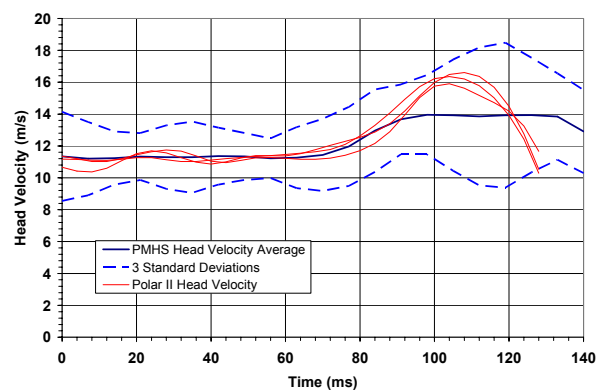


**Figure 16. Dummy head resultant velocity time histories with the average scaled PMHS resultant velocity and 3-standard-deviation corridors.**

The effect on surrogate kinematics as a result of differences in position and differences in height is unknown. More experiments are necessary to assess the affect of differences in height and differences in pre-test orientation on surrogate response.

Despite differences between the response of the PMHS and the dummy, overall PMHS kinematics were generally replicated by the dummy. Dummy trajectories generally fit within 10% path length corridors (Figure 15). Despite the fact that the PMHS trajectories are typically longer, there is a significant difference in the shape of the head trajectory for the dummy and the PMHS.

Although sliding potentially contributes to the difference in shape of the dummy and PMHS head

trajectories, another factor may also contribute to this difference. Without muscle tension in the PMHS, the PMHS neck has very little lateral bending stiffness. The dummy's neck however is designed to replicate the lateral bending stiffness of a living human. This difference is most evident in comparing the high speed video images from the dummy and PMHS tests shown in Figure 6. At 100 and 120 ms, the PMHS neck, due to inertial loading by the head, is under so much bending that it is in contact with the PMHS left shoulder (Figure 6b). However, in the dummy tests, at 100 and 120 ms, the dummy's neck displays much less bending and the closer to being equidistant from each shoulder (Figure 6a).

Differences in head trajectory between the dummy and PMHS are amplified in the resultant head velocity signals. Dummy head velocity is so different from PMHS resultant head velocity signals that dummy resultant head velocity signals barely fit within a three-standard deviation PMHS corridor. The dummy resultant head velocity signals begin to deviate from the scaled average PMHS head velocity around 90 ms. Further analysis of the video data suggests that inertial loading by the head begins to overcome the low stiffness of the PMHS neck around 90 ms. At 80 ms, the PMHS and dummy heads appear to be in a similar place with respect to the shoulders, but at 100 ms, the PMHS neck is under enough lateral bending that the PMHS head is touching the left shoulder (Figure 6). Thus differences in the resultant head velocity between the PMHS and dummy can be at least partially attributed to differences in surrogate neck stiffness.

Since biofidelic representation of living human pedestrians is the ultimate goal in surrogate development, this is an instance when FE modeling could be used to validate the head/neck response of the dummy in a full-scale pedestrian impact test. The motion of T1 could be used as an input to an FE model that has a validated neck muscle model to determine the corresponding head motion.

## CONCLUSION

Three full-scale pedestrian impact tests with PMHS were performed with a late-model small sedan that struck the PMHS at 40 km/h. Three replicate tests were performed with the Polar-II dummy. The kinematics of the Polar-II and PMHS were analyzed by extracting planar body segment parametric trajectory data from high speed video images. A methodology and the necessary data are provided to develop kinematic response corridors for PMHS head, T1, T8 and pelvis trajectories. Trajectory corridors can be calculated based on any  $k$  percent of the path length of the trajectory. The necessary data are also provided to produce the average and standard deviation corridors

for the scaled resultant head velocity measured in the PMHS tests.

Overall, the dummy generally replicated the complex PMHS kinematics and demonstrated good overall biofidelity. Specifically, dummy head, top of thorax, thorax CG and pelvis CG trajectories generally fall within 10% path length corridors. Greater sliding by the PMHS, and lack of neck muscle tension in the PMHS have been identified as potential causes for differences in the length and shape of body segment trajectories. More testing is necessary to assess the effects differences in pre-test orientation, surrogate stature, and clothing will have on surrogate response.

## REFERENCES

- [1] Akiyama A, Okamoto M, Rangarajan N. (2001) Development and application of the new pedestrian dummy. Paper 463, 17th Conference on the Enhanced Safety of Vehicles, Amsterdam, The Netherlands.
- [2] Akiyama A, Yoshida S, Matsushashi T, Moss S, Salloum M, Ishikawa H, Konosu A. (1999a) Development of human-like pedestrian dummy. Paper 9934546, Japanese Society of Automotive Engineers, Chiyoda-Ku, Tokyo, Japan.
- [3] Akiyama A, Yoshida S, Matsushashi T, Rangarajan N, Shams T, Ishikawa H, Konosu A. (1999b) Development of simulation model and pedestrian dummy. Paper 1999-01-0082, Society of Automotive Engineers, Warrendale, PA.
- [4] Artis M, McDonald J, White R, Huang TJ, Shams T, Rangarajan N, Akiyama A, Okamoto R, Yoshizawa R, Ishikawa H. (2000) Development of a new biofidelic leg for use with a pedestrian dummy. Proceedings of the 2000 International Conference on the Biomechanics of Impacts (IRCOBI), Montpellier, France.
- [5] Community Road Accident Database (CARE). EUROPA, European Commission, Transport. [http://europa.eu.int/comm/transport/care/statistics/most\\_recent/detailed\\_breakdown/index\\_en.htm](http://europa.eu.int/comm/transport/care/statistics/most_recent/detailed_breakdown/index_en.htm). 2002. (accessed 15 Apr 2004.)
- [6] Crandall J. (1994) The Preservation of Human Surrogates for Biomechanical Studies. PhD Dissertation released by the University of Virginia Department of Mech and Aero Engineering.
- [7] Huang TJ, McDonald J, Artis M, Rangarajan N, Shams T, White R, Beach D, Campbell R, Akiyama A, Yoshida S, Ishikawa H, Konosu A. (1999) Development of a biofidelic dummy for car-pedestrian accident studies. 1999 International Conference on the Biomechanics of Impacts (IRCOBI), Stiges, Spain.

- [8] Ishikawa H, Kajzer J, Schroeder G. (1993). Computer simulation of the impact response of the human body in car pedestrian crashes. Paper 933129, Proc. 37<sup>th</sup> Stapp Car Crash Conference, 235-248.
- [9] ISO TC 22/SC 22/WG 22. Motorcycles—test and analysis procedures for research evaluation of rider crash protective devices fitted to motorcycles—Part 4: Variables to be measured, instrumentation, and measurement procedures. ISO/DIS 13232-4, August 31, 2004, Copyright ISO, 2004.
- [10] ISO TC 22/SC 22/WG 22. Motorcycles—Test and analysis procedures for research evaluation of rider crash protective devices fitted to motorcycles—Part 5: Injury indices and risk/benefit analysis. ISO/DIS 13232-4, September 7, 2004, Copyright ISO, 2004.
- [11] Kam C, Kerrigan J, Meissner M, Drinkwater C, Murphy D, Bolton J, Arregui C, Kendall R, Ivarsson J, Crandall J, Deng B, Wang JT, Kerkeling C, Hahn W. (2005) Design of a full-scale impact system for analysis of vehicle pedestrian collisions. Paper 2005-01-1875, Society of Automotive Engineers, Warrendale, PA.
- [12] Lessley D, Crandall J, Shaw G, Kent R, Funk J. (2004) A normalization technique for developing corridors from individual subject responses. Paper 2004-01-0288, Society of Automotive Engineers, Warrendale, PA.
- [13] Maltese M, Eppinger R, Rhule H, Donnelly B, Pintar F, Yoganandan N. (2002) Response corridors of human surrogates in lateral impacts. Paper 2002-22-0017, Society of Automotive Engineers, Warrendale, PA.
- [14] Okamoto Y, Akiyama A, Okamoto M, Kikuchi Y. (2001) A study of the upper leg component tests compared with pedestrian dummy tests. Paper 380, 17th Conference on the Enhanced Safety of Vehicles (ESV), Amsterdam, The Netherlands.
- [15] Robbins DH. Anthropometric Specifications for Mid-Sized Male Dummy, Volume 2. University of Michigan Transportation Research Institute (UMTRI) report number UMTRI-83-53-2. December 1983.
- [16] National Highway Traffic Safety Administration. (2003) Traffic Safety Facts 2003-Pedestrians, DOT HS 809 769, 2003.
- [17] National Police Agency (Japan). Traffic Accidents Situation 2003. Fatalities by Age Group and Road User Type. <http://www.npa.go.jp/english/index.htm>. 2003. (Accessed 12 Apr. 2004.)
- [18] Viano D, Davidsson J. (2002) Neck displacements of volunteers, BioRID P3 and Hybrid III in rear impacts: implications to whiplash assessment by a neck displacement criterion (NDC). Traffic Injury Prevention 3: 105-116.
- [19] World Bank (2001) Road Safety. <http://www.worldbank.org/transport/roads/safety.htm> (Accessed 12 Apr. 2004).